University of Texas Rio Grande Valley

ScholarWorks @ UTRGV

Earth, Environmental, and Marine Sciences
Faculty Publications and Presentations

College of Sciences

10-7-2019

Broadband sound propagation in a seagrass meadow throughout a diurnal cycle

Kevin M. Lee
University of Texas at Austin, kevin.lee@arlut.utexas.edu

Megan S. Ballard
University of Texas at Austin, meganb@arlut.utexas.edu

Gabriel R. Venegas
University of Texas at Austin, gvenegas@utexas.edu

Jason D. Sagers
University of Texas at Austin, sagers@arlut.utexas.edu

Andrew R. McNeese
University of Texas at Austin, mcneese@arlut.utexas.edu

Recommended Citation

Authors

Kevin M. Lee, Megan S. Ballard, Gabriel R. Venegas, Jason D. Sagers, Andrew R. McNeese, Jay R. Johnson, Preston S. Wilson, and Abdullah Rahman

Broadband sound propagation in a seagrass meadow throughout a diurnal cycle

**Kevin M. Lee,[1,a)] Megan S. Ballard,[1] Gabriel R. Venegas,[1]
Jason D. Sagers,[1] Andrew R. McNeese,[1] Jay R. Johnson,[2]
Preston S. Wilson,[2,b)] and Abdullah F. Rahman[3]**

[1]*Applied Research Laboratories, University of Texas at Austin, Austin, Texas 78713, USA*
[2]*Walker Department of Mechanical Engineering, University of Texas at Austin, Austin, Texas 78712, USA*
[3]*School of Earth, Environmental, and Marine Sciences, University of Texas Rio Grande Valley, Brownsville, Texas 78520, USA*
kevin.lee@arlut.utexas.edu, meganb@arlut.utexas.edu, gvenegas@utexas.edu,
sagers@arlut.utexas.edu, mcneese@arlut.utexas.edu, johnson.jayrichard@utexas.edu,
pswilson@mail.utexas.edu, abdullah.rahman@utrgv.edu

Abstract: Acoustic propagation measurements were conducted in a *Thalassia testudinum* meadow in the Lower Laguna Madre, a shallow bay on the Texas Gulf of Mexico coast. A piezoelectric source transmitted frequency-modulated chirps (0.1 to 100 kHz) over a 24-h period during which oceanographic probes measured environmental parameters including dissolved oxygen and solar irradiance. Compared to a nearby less vegetated area, the received level was lower by as much as 30 dB during the early morning hours. At the peak of photosynthesis-driven bubble production in the late afternoon, an additional decrease in level of 11 dB was observed.
© 2019 Acoustical Society of America
[DRB]
Date Received: August 1, 2019   **Date Accepted:** August 29, 2019

1. Introduction

Seagrasses are ubiquitous along coastlines across the globe, ranging from tropical to temperate regions, and with approximately 50 distinct species in existence worldwide, they perform a multitude of vital marine ecosystem services, including nutrient cycling and sediment stabilization, supporting habitat biodiversity, and carbon sequestration.[1] Therefore, it is concerning that global seagrass coverage is declining at a median rate of 7% yr^{-1} (since 1990) partially due to anthropogenic causes such as destructive fishing practices, coastal engineering, pollution, and climate change.[2]

Seagrasses, like terrestrial angiosperms, produce oxygen via photosynthesis. When the partial pressure of oxygen contained in the lacunae (gas bodies within the plant) exceeds that of the surrounding water, oxygen diffuses through the plant tissue to form bubbles on the surfaces of the leaves. Oxygen is also transferred continually to the rhizosphere (the sediment surrounding the rhizomes and roots) due to generally hypoxic conditions in the sediment and at varying rates based on photosynthesis and respiration. Gas volumes produced by all of these processes have implications for underwater acoustic propagation in coastal regions where seagrass is present since it is known that bubbles in liquid, biological tissue, or sediment lead to the dispersion, absorption, and scattering of sound.[3–6]

Previous work identified the potential to exploit the sensitivity of acoustic waves to photosynthesis bubbles as biophysical markers to assess seagrass ecosystem health. Hermand conducted pioneering experiments on acoustic sensing of photosynthesis by the Mediterranean seagrass species *Posidonia oceanica*.[7–9] The first experiment of Hermand *et al.* established a causal relationship between photosynthesis daily cycle and variation in attenuation and time dispersion characteristics in a shallow water waveguide using low-frequency broadband (0.1–1.6 kHz) propagation experiments in dense *P. oceanica* meadow.[7] Preliminary modeling indicated that the inverse problem of determining gas and oxygen void fraction in the bottom seagrass layer could be solved, and Hermand suggested that seagrass density and photosynthetic activity could potentially be derived from inverted void fractions. A second experiment was conducted with a broader frequency band (0.2–16 kHz) in a lower density Posidonia bed that had much lower oxygen productivity, and a similar dependence on variation of

---

[a)]Author to whom correspondence should be addressed.
[b)]Also at: Applied Research Laboratories, University of Texas at Austin, Austin, Texas 78713, USA.

waveguide impulse response with photosynthetic activity was demonstrated.[8,9] More recently, Felisberto *et al.* deployed an autonomous experiment in a *P. oceanica* meadow, in which they demonstrated a high degree of correlation between the received acoustic energy and the estimated water column oxygen bubble concentration, which was derived from dissolved oxygen measurements.[10] In this study, the authors looked at three frequency bands (0.4–0.8, 1.5–3.5, 6.5–8.5 kHz) and found that perturbations in the received energy in the two lower bands were more sensitive to oxygen concentration than the higher band. Additionally, they found that variability in the modal interference patterns was highest during the day during photosynthetic activity, both in their field experiment and in tank experiments with *Cymodocea nodosa*.[11] Finally, a study was conducted on acoustic sensing of photosynthesis with three Atlantic seagrass species (*Syringodium filiforme*, *Halodule wrightii*, and *Thalassia testudinum*), but the experiment was conducted in outdoor tanks and at a single frequency of 100 kHz.[12] In this case, a positive correlation was found between received acoustic energy at this frequency and photosynthetically active radiation for *S. filiforme*, negative correlation for *H. wrightii*, and no correlation for *T. testudinum*.

This letter reports *in situ* measurements of the waveguide impulse response in a dense *T. testudinum* meadow throughout a complete diurnal cycle. Environmental parameters such as dissolved oxygen, water temperature, wind speed, water depth, and solar irradiance were monitored throughout the duration of the acoustic measurements. The goals of the work reported in this letter were to: (1) determine the diurnal dependence of acoustic propagation in a *T. testudinum* meadow as a function of oxygen concentration, (2) use wideband excitation (1–100 kHz) to determine the limits of the frequency band that is most affected by changes in the oxygen concentration, and (3) perform measurements in a nearby sandy area with a much lower density of seagrass for direct comparison to the dense seagrass bed. Most of the previous *in situ* work has focused on the Mediterranean species *P. oceanica*, and the only previous work with Atlantic species was conducted in outdoor mesocosms with plants removed from the field.[12] Also in contrast to previous work, the frequency band used here is much broader—the earlier Posidonia work was conducted within the 0.1–16 kHz band, and the Atlantic species tank experiments were at a single frequency of 100 kHz. Finally, a comparison of the seagrass measurements with those taken in the nearby relatively seagrass-free area allows for a baseline estimate of the effect of seagrass on the propagation environment in the absence of photosynthesis bubbles during the early morning hours. No previous work offered such a comparison.

2. Propagation experiment

The experiment was conducted in the Lower Laguna Madre, part of a hypersaline lagoon system on the southern Texas Gulf of Mexico coast, during October 2–4, 2018. The seagrass beds of Lower Laguna Madre are representative of the entire Tropical Atlantic seagrass bioregion.[1] *T. testudinum* is the most abundant species in this area; however, small groupings of *H. wrightii* and *S. filiforme* are scattered throughout the meadow.[13] In early October, *T. testudinum* is typically just past the annual peak of its above-ground biomass for that geographical region,[13] and the canopy extends 30 cm or more into the water column from the lagoon bed, forming dense meadows interspersed with barren patches ranging from a few meters to several hundred meters in diameter. The water depth where the experiment was conducted ranged from approximately 1 to 1.5 m, depending on the tide. Acoustic measurements were taken at two distinct locations in the lagoon: a site inside the seagrass meadow (26° 6.340′ N, 97° 10.491′ W) and a large less vegetated patch to the north (26° 9.054′ N, 97° 11.068′ W) with an overall area of roughly 50 000 m². Representative photographs from the two sites near the locations that the acoustic transducers were stationed are shown in Figs. 1(a) and 1(b).

2.1 Acoustic measurements

A piezoelectric sound source and three hydrophones were deployed at each measurement site. The hydrophones were positioned along a line at horizontal distances from the source of 1.5, 3, and 6 m. The acoustic centers of the source and hydrophones were located 20 and 10 cm above the lagoon floor, respectively, such that all the transducers were within the canopy at the seagrass site. The vertical placement of the transducers was chosen in part to avoid damage by propellers of small watercraft in the vicinity. A schematic of the experimental configuration is shown in Fig. 1(c).

The excitation signal was a frequency-modulated chirp with a bandwidth of 0.1 to 100 kHz and a duration of 50 ms. An exponential chirp was chosen, given by the function
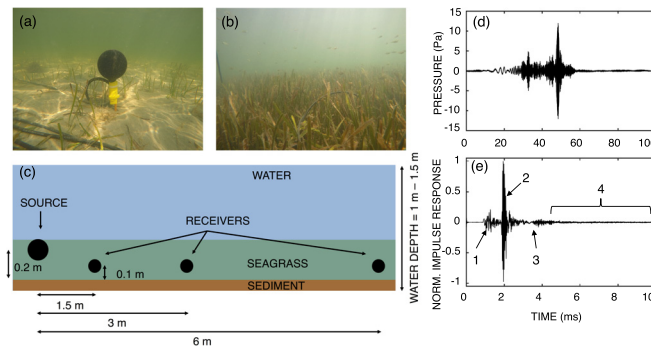
Fig. 1. (Color online) Underwater photographs of the (a) bare (low vegetation density) and (b) seagrass (high vegetation density) experiment sites. The sound source is visible in (a). (c) Schematic of the experiment geometry. (d) Raw received chirp signal on the receiver 1.5 m away from the source. (e) Computed impulse response for the same signal shown in (d). The following features are indicated in (e): (1) direct path and first bottom interaction, which are separated by less than 1 ms, (2) first surface reflection, (3) surface-bottom-surface reflection, and (4) long reverberant tail with higher-order multipath reflections.

$$ s(t) = A(t) \sin \left[\frac{\omega_1 t_0}{\ln\left(\frac{\omega_2}{\omega_1}\right)} \left\{ \exp\left[\frac{t}{t_0} \ln\left(\frac{\omega_2}{\omega_1}\right) \right] - 1 \right\} \right], \tag{1} $$

where t_0 is the length of the chirp in seconds, ω_1 is the beginning angular frequency, and ω_2 is the ending angular frequency. Selection of this chirp function ensured that a greater amount of time was spent transmitting at frequencies below the source transducer resonance (near 18 kHz) where the source output was lower to improve the signal-to-noise ratio in that band. Additionally, the amplitude of the chirp $A(t)$ was weighted to counteract the frequency response of the source such that ringing at resonance would be minimized. The signal was passed through a power amplifier to the source transducer, which emitted an acoustic pulse that propagated through the shallow-water waveguide and was received at each of the three hydrophones. Sixteen chirps were transmitted at 2-s intervals and averaged, and this sequence was repeated approximately every 10 min over a full 24-h period for a total 138 transmission events. The drive voltage provided by the power amplifier was monitored over the entire experiment, with a variation of less than 0.008 dB relative to the root-mean-square level averaged over all pings. An example of a raw chirp signal received at the hydrophone 1.5-m away from the source at the seagrass site is shown in Fig. 1(d). The excitation signal had a time-bandwidth product of nearly 5000, allowing for sufficient pulse compression such that multipath arrivals could partially be resolved in time at the closest source/receiver separation distance by applying deconvolution techniques. The received signal from each hydrophone was then convolved with an inverse filter to obtain a band limited impulse response, which contains both the waveguide impulse response, the responses of the source and the receiver, and any additive ambient noise that is present.[14] Figure 1(e) shows the post-processed impulse response corresponding to the raw signal in Fig. 1(d) with arrivals corresponding to various propagation paths indicated.

2.2 Environmental measurements

An autonomous data logger was deployed adjacent to the acoustic experiment to measure water temperature and dissolved oxygen in regular 2 min intervals. Several seawater samples were collected throughout the experiment, and the salinity was measured using a handheld refractometer. Cores collected from a nearby area in the seagrass meadow were analyzed to compare sediment properties both underneath the seagrass and in the seagrass-free patches.[15] Solar irradiance was logged throughout the daylight hours with a blackbody thermopile pyranometer. The pyranometer was sensitive at electromagnetic wavelengths ranging from 385 to 2105 nm, which is inclusive of the photosynthetically active radiation band.[16] A nearby weather buoy operated by the National Data Buoy Center, located at station PCGT2 (26° 4.32′ N, 97° 10.02′ W), provided tide level and wind speed data. The tide level data, which was available in 6 min increments, was then calibrated to water depth at the experiment site with measurements obtained by manually sampling the water depth using a ruler at various times throughout the experiment.

3. Results and discussion

Temporal dependence of solar irradiance, dissolved oxygen, and the received impulse responses measured at the closest and farthest receivers from the source are shown in Fig. 2. After the start of the experiment, the solar irradiance decreased with the setting

sun until the measured value was within the self-noise of the pyranometer at nightfall ($<45\,\mathrm{W/m^2}$); therefore, irradiance readings were not recorded during the hours of darkness (shaded regions in Fig. 2). After sunrise, solar irradiance increased to a maximum of $893\,\mathrm{W/m^2}$, which occurred at 12:58 on October 3, 2018, after which it began to decrease again heading toward sunset.

Dissolved oxygen content was used as a proxy measurement for the void fraction of photosynthesis bubbles produced by the plants in the water column. At the beginning of the experiment, the dissolved oxygen content was 160%, and bubbles were also observed adhering to the leaves of the plants and rising freely in the water column. Values of dissolved oxygen greater than 100% indicate that the seawater is supersaturated. After sunset, the dissolved oxygen content steadily decreased overnight, crossing under the 100% saturation level at 1:23 in the early morning and reaching a minimum value of 51% at 7:44, shortly after daybreak. As the seagrass began to release oxygen into the water column, the dissolved oxygen content rose, crossing over the 100% saturation threshold at 12:18 and reaching a maximum at shortly before sunset. Around the same time the dissolved oxygen content surpassed saturation level, bubbles were again observed on leaves of the seagrass and were seen rising in the water column throughout the remainder of the experiment. The wind speed over the 24-h period of the experiment was low (less than 10 knots), displaying little dependence on time of day, and no breaking waves were observed. Therefore, oxygen bubbles introduced into the water column by the seagrass was assumed to be the primary contributor to the dissolved oxygen content measured during the experiment.

The impulse responses measured on the receivers closest and farthest to the source are shown in Figs. 2(c) and 2(d). To elucidate the observed time-varying arrival structure, the estimated arrival times of the first few propagation paths are indicated by the colored lines. Over the duration of the experiment, the salinity was measured from water samples at 36 ± 1 psu, the uncertainty being limited by the refractometer's reticule, the mean water temperature was $30.3 \pm 1.1\,^\circ\mathrm{C}$, in which the uncertainty is given by the standard deviation of the water temperature data logger measurements, and the corresponding background seawater sound speed at 1 m water depth was $1547 \pm 2\,\mathrm{m/s}$.[17] Using the mean value of sound speed, the water-depth time-record, and the geometry of the transducer deployment shown in Fig. 1(c), the arrival times for various propagation paths at each of the receivers were estimated as a function of time of day. The time-dependence of the two surface-interacting arrivals is primarily due to tidal changes in the water depth. Because the direct path and first bottom reflection do not interact with the water surface, these arrival times do not display tidal variation. The temporal dependence of the amplitude of the arrival most closely associated with the direct path/bottom reflection arrival pair on the 1.5 m range receiver exhibits a relationship to the dissolved oxygen level with lower amplitudes corresponding to times with higher levels of dissolved oxygen content. There is a similar variation in the other arrivals; however, it is difficult to discern this
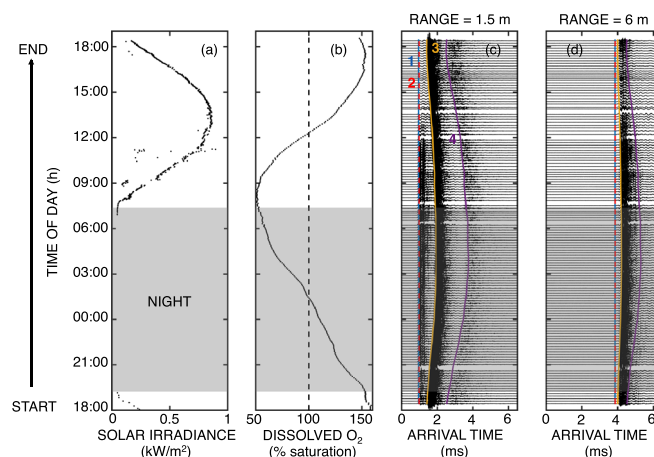

Fig. 2. (Color online) Dependence of (a) solar irradiance, (b) dissolved oxygen, and acoustic arrivals at source/receiver ranges of (c) 1.5 m and (d) 6 m. The gray-shaded regions in all panels indicate night (sunset to sunrise). The dashed vertical line in (b) denotes 100% saturation of dissolved oxygen in seawater. The vertical lines in (c) and (d) designate the following acoustic arrivals: direct path (1, solid line), first bottom reflection (2, dashed line), first surface bounce (3), and the surface-bottom-surface arrival (4). Note that the curve representing the first bottom reflection lies nearly on top of the direct path. The start of the experiment was shortly before sunset on October 2, 2018, and the end of the experiment was at sunset the following day. Gaps in the acoustic record occurred a few times when the data acquisition system was stopped and restarted.

given the scale used in Fig. 2(c). At the 6 m range receiver shown in Fig. 2(d), all of the arrivals overlap, but the overall amplitude of the resultant interference pattern has temporal dependence that qualitatively appears inversely proportional to dissolved oxygen content. For the remaining analysis, the data from the 6 m range receiver are used because it represents the longest propagation path and hence has the most interaction with the environment.

To quantify the temporal dependence of the waveguide impulse response, the received acoustic energy is plotted as a function of time of day in Fig. 3(a) for both the seagrass bed and the bare patch. Superimposed on this plot are dissolved oxygen levels measured at both sites. The received acoustic energy was estimated by computing the integral

$$E = \int_T h(t)^2 dt, \qquad (2)$$

where $h(t)$ is the impulse response measured on the farthest hydrophone and T is a time interval that encompasses the received signal. For the numerical integration, a window length of 4 ms was used. Most of the signal energy was included in this window as it was found that increasing the window length had very little effect on the resultant level. The levels are normalized such that mean value near dawn is set to 0 dB. After the start of the experiment (October 2, 2018, 18:26), the received level increases steadily until the dissolved oxygen approaches 120%, with an overall increase in acoustic energy from the start of the experiment of approximately 6 dB. Presumably bubble production has ceased by this time (21:00), but there is a lag in the response of the dissolved oxygen content. The received energy level remains constant to within ±2 dB throughout the rest of the night and into the morning until the dissolved oxygen content again surpasses 100% in the early afternoon at 12:18, after which the level steadily decreases to a final value of approximately −11 dB. The overall change in the acoustic amplitude between the late afternoon on both October 2, 2018 and October 3, 2018 and the early morning is attributed to the production of free oxygen bubbles in the water column by photosynthesis. Because of the very shallow nature of this waveguide, changes in water depth due to the tidal cycle present significant changes to the water depth (as much as 50%); however, contributions to the overall attenuation from variation in transmission path length in the water layer are expected to be small compared to effects of the bubbles and gas bodies within the plants. Data collected in the bare patch (October 4, 2018, 9:15–11:36) are also shown in Fig. 3(a); however, a negative 30 dB offset was applied to this data to align it with the maximum levels measured in the seagrass bed. The dissolved oxygen content in the bare patch is similarly low compared to that of near-dawn hours in the seagrass bed, and the 30 dB difference in peak level between the bare patch and the seagrass bed is attributed to the presence of the gas bodies encapsulated within the plants themselves since photosynthesis bubbles were not present in significant amounts during the morning hours at either location. Surficial sediment properties that are representative
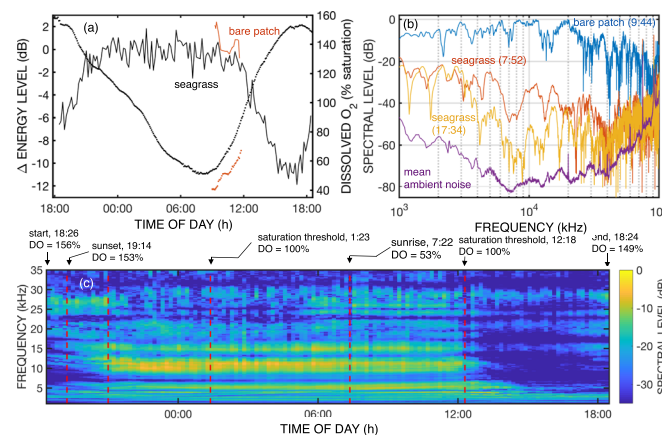

Fig. 3. (Color online) (a) Changes in received acoustic energy (solid lines, left horizontal axis) and dissolved oxygen (circles, right horizontal axis) vs time of day. Data are shown for the seagrass bed and the bare patch. To place the bare patch data on the same scale as the seagrass data, a horizontal offset of 24 h was applied to all of the bare patch data, and a vertical offset of −30 dB applied to the bare patch acoustic data. (b) Spectral levels for the bare patch (time of day = 9:44, dissolved oxygen = 41%), seagrass bed early in the morning (time of day = 7:52, dissolved oxygen = 51%) and late afternoon (time of day = 17:34, dissolved oxygen = 152%), and mean ambient noise level in the seagrass bed for the 24 h experiment period. (c) Time history of spectral levels in seagrass bed. Dissolved oxygen levels (DO) are indicated for various times of day throughout the experiment.

Table 1. Summary of representative sediment properties underneath the seagrass and in the bare patch. Values are averaged over the top 40 cm of the sediment. Details of the core processing are given in Venegas *et al.* (Ref. 15).

	Porosity	Mean Grain Size (ϕ)	% Sand	% Silt	% Clay	% C_{org}
Seagrass bed	0.59	4.7	51	30	18	2.1
Bare patch	0.46	3.8	70	17	12	0.9

of the seagrass bed and the bare patch, including total organic carbon (C_{org}), are listed in Table 1. Although the sediment types and organic carbon content from the two areas are not identical, these differences alone are not enough to explain the difference in received energy in the water column measured between the two sites.

A comparison of spectral levels between the bare patch and the seagrass bed at different times of day is shown in Fig. 3(b). A Blackman–Harris window was first applied to each impulse response to improve side lobe suppression prior to taking the Fourier transform. Then, the spectra were corrected for the measurement system frequency response, which was obtained from free-field measurements collected in a bubble-free calibration tank. The difference in 1–100 kHz band-averaged level between the bare patch and early morning seagrass data is 25 dB, and the level differences between the two cases at 1 and 10 kHz are 9 and 33 dB, respectively. Above 80 kHz, the seagrass data are coincident with the mean ambient noise floor in the seagrass bed, which was computed from ambient noise data collected over the entire 24 h period. The late afternoon seagrass data displays excess attenuation in the 3.5 to 35 kHz band compared to the early morning data, and the maximum difference of 21 dB between the two cases occurs in the one-third octave band centered at 10 kHz. Using the Minnaert equation[18]

$$R_0 = \sqrt{\frac{3\gamma p}{\rho \omega_0^2}}, \qquad (3)$$

the center frequency $\omega_0/2\pi = 10$ kHz, and nominal values for seawater density ($\rho = 1029$ kg/m^3) and the ratio of specific heats of oxygen ($\gamma = 1.4$), an estimate of the bubble diameter at hydrostatic pressure p corresponding to 1 m water depth is approximately $2 R_0 = 0.7$ mm, which is qualitatively consistent with observations made of bubbles attached to the seagrass leaves during the field experiment when the seagrass was photosynthetically active in the afternoon. Use of Eq. (3) is a lowest order approximation for understanding the observed acoustic effects. Pressurization of the gas bodies within the plants depends on photosynthetic activity, and hence changes throughout the day. More complex multiphase models that include both free bubbles and encapsulated gas bodies within the plants are needed to explain the full behavior; however, such models do not yet exist.

Finally, the complete time history of spectral levels recorded in the seagrass bed is shown in Fig. 3(c), in which the frequency axis is centered on the 1 to 35 kHz band. By 21:00 (dissolved oxygen content = 132%), the mean spectral level in the 3.5 to 35 kHz band increases to within 1 dB of the mean spectral level obtained when the dissolved oxygen content falls beneath 100% at 1:23 later that night, indicating that bubble production has ceased by the earlier time. Some reduction in level is observed in the 23 to 28 kHz band from between 21:00 and 5:00, but this could be due to other biological or non-biological processes, the cause of which is not yet determined. Overall, however, the spectral nulls do not vary greatly through the night and morning hours, indicating that the effective sound speed in the medium is relatively stable during this time, which would be expected if the medium has a time-invariant void fraction. Excess attenuation in the 3.5 to 35 kHz band returns once bubble production resumes and the dissolved oxygen content crosses the saturation threshold at 12:18. The excess attenuation persists throughout the remainder of the experiment.

4. Conclusions

This letter reports *in situ* acoustic measurements of photosynthesis in a bed of *T. testudinum*. All previously reported *in situ* acoustic measurements of seagrass photosynthesis in natural environments were with *P. oceanica*; however, not all seagrass species produce O$_2$ at the same rate, making observation of many species important to establishing the robustness of acoustic monitoring techniques. Photosynthesis leads to the formation of free bubbles in the water column when the dissolved oxygen content reaches saturation conditions. A reduction of nearly 11 dB in received acoustic energy was observed between sunrise and sunset. The use of a wider band of excitation (1–100 kHz) than previous

experiments allowed for identification of an excess attenuation band that occurred from 3.5 to 35 kHz in the afternoon when bubble production was at a maximum; however, these acoustic levels recover at night when photosynthesis ceases. Another new contribution of this work is the comparison of propagation in a seagrass bed with a nearby area with significantly less seagrass coverage. The received acoustic energy level was 30 dB lower in the seagrass compared to the close-by, nearly seagrass-free area.

The ultimate goal of this experiment and the previous work[7–12] is to use acoustics to monitor seagrass oxygen production on the scale of a meadow. Inference of oxygen production from acoustic propagation measurements will require an accurately parameterized propagation model as well as an established relationship between the inferred bubble size distribution and productivity. Results from this and other similar experiments will provide data to aid in developing the acoustic propagation models, hopefully for a variety of propagation environments and seagrass species. Future work will examine variability of acoustic behavior over several consecutive diurnal cycles and look at seasonal dependence.

Acknowledgments

References and links

[1] F. Short, T. Carruthers, W. Dennison, and M. Waycott, "Global seagrass distribution and diversity: A bioregional model," J. Exp. Mar. Biol. Ecol. **350**, 3–20 (2007).

[2] M. Waycott, C. M. Duarte, T. J. B. Carruthers, R. J. Orth, W. C. Dennison, S. Olyarnik, A. Calladine, J. W. Fourqurean, K. L. Heck, Jr., A. R. Hughes, G. A. Kendrick, W. J. Kenworthy, F. T. Short, and S. L. Williams, "Accelerating loss of seagrasses across the globe threatens coastal ecosystems," Proc. Nat. Acad. Sci. U.S.A. **106**, 12377–12381 (2009).

[3] D. L. Miller, "A cylindrical-bubble model for the response of plant-tissue gas bodies to ultrasound," J. Acoust. Soc. Am. **65**, 1313–1321 (1979).

[4] K. W. Commander and A. Prosperetti, "Linear pressure waves in bubbly liquids: Comparison between theory and experiments," J. Acoust. Soc. Am. **85**, 732–746 (1989).

[5] X. Yang and C. C. Church, "A model for dynamics of gas bubbles in soft tissue," J. Acoust. Soc. Am. **118**, 3595–3606 (2005).

[6] H. Dogan, P. R. White, and T. G. Leighton, "Acoustic wave propagation in gassy porous marine sediments: The rheological and the elastic effects," J. Acoust. Soc. Am. **141**, 2277–2288 (2017).

[7] J. P. Hermand, P. Nascetti, and F. Cinelli, "Inverse acoustical determination of photosynthetic oxygen productivity of Posidonia seagrass," in *Experimental Acoustic Methods for Exploration of Shallow Water Environment* (Kluwer Academic Publishers, Netherlands, 2000), pp. 125–144.

[8] J. P. Hermand, "Acoustic remote sensing of photosynthetic activity in seagrass beds," in *Handbook of Scaling Methods in Aquatic Ecology: Measurement, Analysis, Simulation* (CRC Press, Boca Raton, FL, 2004), pp. 65–96.

[9] J. P. Hermand, "Continuous acoustic monitoring of physiological and environmental processes in seagrass prairies with focus on photosynthesis," in *Acoustic Sensing Techniques for the Shallow Water Environment* (Springer, Netherlands, 2006), pp. 183–196.

[10] P. Felisberto, S. M. Jesus, F. Zabel, R. Santos, J. Silva, S. Gobert, S. Beer, M. Björk, S. Mazzuca, G. Procaccini, J. W. Runcie, and W. Champenois, "Acoustic monitoring of O_2 production of a seagrass meadow," J. Exp. Mar. Biol. Ecol. **464**, 75–87 (2015).

[11] P. Felisberto, O. C. Rodríguez, J. ao Silva, S. M. Jesus, H. Q. Ferreira, P. P. Ferreira, M. E. Cunha, C. B. de los Santos, I. Olivé, and R. Santos, "Monitoring bubble production in a seagrass meadow using a source of opportunity," Proc. Mtgs. Acoust. **30**, 005002 (2017).

[12] C. J. Wilson, P. S. Wilson, and K. H. Dunton, "An acoustic investigation of seagrass photosynthesis," Mar. Biol. **159**, 2311–2322 (2012).

[13] J. E. Kaldy and K. H. Dunton, "Above- and below-ground production, biomass, and reproductive ecology of *Thalassia testudinum* (turtle grass) in a subtropical coastal lagoon," Mar. Ecol. Prog. Ser. **193**, 271–283 (2000).

[14] A. J. Berkhout, D. de Vries, and M. M. Boone, "A new method to acquire impulse responses in concert halls," J. Acoust. Soc. Am. **68**, 179–183 (1980).

[15] G. R. Venegas, A. F. Rahman, K. M. Lee, M. S. Ballard, and P. S. Wilson, "Toward the ultrasonics sensing of organic carbon in seagrass-bearing sediments," Geophys. Res. Lett. **46**, 5968–5977, https://doi.org/10.1029/2019GL082745 (2019).

[16] R. C. Zimmerman, "Light and photosynthesis in seagrass meadows," in *Seagrasses: Biology, Ecology, and Conservation*, edited by A. W. D. Larkum, R. J. Orth, and C. M. Duarte (Springer, Dordrecht, Netherlands, 2006), Chap. 13, pp. 303–321.

[17] L. E. Kinsler, A. R. Frey, A. B. Coppens, and J. V. Sanders, *Fundamentals of Acoustics*, 4th ed. (John Wiley & Sons, Inc., New York, 1999), p. 436.

[18] T. G. Leighton, *The Acoustic Bubble* (Academic Press, London, 1994), p. 139.